International Journal of Satellite Communications and Networking

WILEY

ORIGINAL PAPER OPEN ACCESS

CLEAR Interference Cancellation in a Wideband Dual-Channel Receiver for Independent Satellite Multi-Connectivity Links

Svilen Dimitrov

Satellite Networks Department, German Aerospace Center (DLR), Wessling, Germany

Correspondence: Svilen Dimitrov (svilen.dimitrov@dlr.de)

Received: 24 February 2026 | **Revised:** 4 May 2026 | **Accepted:** 6 May 2026

Keywords: 5G NTN | CCSDS | co-channel interference (CCI) | correlation learning estimation and adaptive reduction (CLEAR) | cross-polarization interference (XPI) | dual-channel receiver | DVB-S2X | energy efficiency | higher order modulation | multi-connectivity | polarization division multiplexing (PDM) | satellite communications

ABSTRACT

In this paper, the correlation learning estimation and adaptive reduction (CLEAR) of interference, an adaptive, blind and transparent interference compensation method applied in a wideband dual-channel receiver, is studied for a pair of independent satellite multi-connectivity links, using the same carrier frequency and signal bandwidth in use cases with or without polarization division multiplexing (PDM). The CLEAR method jointly processes the samples of the two channels after the corresponding analog-to-digital converters (ADCs), it has a low computational complexity and is suitable for very-high-rate implementations. This non-data-aided and non-decision-directed method is derived in a channel model with co-channel interference (CCI) and/or cross-polarization interference (XPI), including effects such as reduced cross-channel discrimination (XCD) and/or cross-polarization discrimination (XPD) of the receive antenna, depolarization due to atmospheric conditions, differential frequency offset (DFO) between the two channels, and power imbalance due to independent receive antenna gains. The resulting carrier-to-interference ratio C/I and carrier-to-noise-and-interference ratio $C/(N+I)$ performance of the dual-channel receiver presents considerable energy efficiency improvements with this interference compensation method, and is particularly beneficial for higher-order modulation. As a result, the CLEAR method is a practical solution to increase the data rates of the satellite air interface in DVB-S2X/CCSDS and 5G NTN systems by the use of two independent satellite links.

1 | Introduction

Satellite communications have experienced a significant growth in recent years. The total number of active satellite payloads in low-Earth orbit (LEO) is projected to reach more than 60,000 by 2030 [1] from 11,000 in 2024 [2], driven by the rapid expansion of commercial mega-constellations, for example, SpaceX Starlink, Amazon Kuiper, and the European IRIS$_2$ initiative. Customary satellite applications such as digital satellite television, professional satellite networks, and global internet access over geostationary-Earth-orbit (GEO) satellites, as well as Earth observation with LEO satellites, utilize an air interface with DVB-S2X [3] and CCSDS [4] waveforms. Due to the pivotal role of providing global coverage, satellite networks have nowadays been recognized as an integral part of 5G and upcoming 6G communications and designated as non-terrestrial networks (NTNs). For the purpose of seamless integration with terrestrial networks (TNs), the satellite links have adopted an air interface with New Radio (NR) waveforms based on orthogonal frequency division multiplexing (OFDM) [5], and the service has been taken over by constellations of LEO satellites due to their inherent shorter transmission paths with lower latency.

A number of satellite applications require high data rates over large bandwidths, for example, gateway feeder links, wideband user/service links for professional applications, and satellite downlinks for Earth observation. Due to the limitation of the available radio frequency (RF) spectrum, simultaneous transmission from two independent satellites to a single location on ground equipped with a dual-channel receiver [6, 7], using the same carrier frequency and the same signal bandwidth, can double the data rate of such wideband communication links. This scenario is supported by the proposed satellite multi-connectivity over regenerative or transparent LEO payloads with Earth-fixed beams in 5G NTN [8]. One way to practically realize this setup is to use a single dual-polarization antenna at the receiver side on ground, capable of simultaneous communications on two orthogonal antenna polarizations with polarization division multiplexing (PDM), and the respective single-polarization antennas on board the two independent satellites. Alternatively, two co-located single-polarization antennas can be deployed on ground, where the cross-channel discrimination (XCD) is provided either by the different gains in the direction of the two satellites of the two receive antenna patterns using the same polarization, or by PDM with different polarizations on the two links, or both. Here, the different slant range with resulting different path loss and/or the antenna gains on the two links can lead to different received power of the signals on the two channels. In addition, in the case with PDM, imperfections of the receive antennas, as well as effects of the atmosphere caused by water droplets and ice crystals, reduce the cross-polarization discrimination (XPD) and degrade the orthogonality of the two polarizations. The increased co-channel interference (CCI) and/or cross-polarization interference (XPI) between the two channels, resulting from the reduced XCD and/or XPD, reduces the carrier-to-interference ratio C/I and, as a result, the carrier-to-noise-and-interference ratio $C/(N+I)$ at the receiver which degrades the performance of the demodulator and decoder. In state-of-the-art LEO-satellite systems [3–5], adaptive coding and modulation (ACM) is employed to adjust the modulation format according to the elevation-dependent, and therefore time-variable, interference and the resulting $C/(N+I)$ conditions during the satellite visibility window. High CCI and/or XPI are, therefore, a limiting factor for the application of higher order modulation formats and the achievable data rates. In order to mitigate the effects of this time-variable interference, an adaptive receiver algorithm performing interference estimation and cancellation is required. In addition to the CCI and/or XPI, differential frequency offset (DFO) is introduced between the two independent channels at the receiver when using two independent voltage-controlled oscillators (VCOs) in the downconversion blocks of the two channels due to instabilities. Therefore, the CCI and/or XPI compensation algorithm needs to be able to operate in the presence of the DFO, since the DFO is an inherent feature of the signal in the channel which is used for interference estimation and cancellation.

Proprietary solutions to compensate the XPI in a DVB-S2X [3] and CCSDS [4] receiver are based on symbol-spaced or fractionally-spaced adaptive filter architectures with access to the signals on both polarizations, for example, the cross-polarization digital equalization and automatic filtering (XDEAF) method [9] which is closely related to XPI cancellation (XPIC) [10]. The training of the filter coefficients can be data-aided by means of known pilot symbols or decision-directed, that is, blind, requiring knowledge of the used modulation format at the receiver. An extension to the XPIC method for operation with DFO between the two channels has been presented in [11], including additional electronic components at the expense of higher receiver complexity. The performance of the decision-directed approach is severely penalized for higher-order modulation in Gaussian noise, while the data-aided approach results in a very large pilot overhead in the presence of DFO due to the required very frequent XPI estimation and cancellation [6, 7] countered by the slow convergence of filter coefficients training [10]. In addition to proactive ACM, successive interference cancellation (SIC) and cooperation between the two satellites at the cost of increased system complexity have been discussed in [12]. Space-time coding and spatial modulation have also been presented for dual-polarized mobile satellite communications [13, 14]. For their successful demodulation, however, these solutions also require data-aided provision of channel state information at the receiver (CSIR), as well as joint processing of the two signals at the transmitter side with stringent timing and frequency synchronization requirements which is practically challenging in the scenario with two independent satellites. In 5G NTN, joint processing of the signals at the transmitter side is used for massive multiple-input-multiple-output (MIMO) communications [15], allowing the reuse of large bandwidths to multiple users via beamforming within the beam. While this can be applied individually in each satellite, joint signal processing across two independent satellites is also an issue.

In this paper, the previously presented correlation learning estimation and adaptive reduction (CLEAR) of interference [6, 7] is proposed for application in a wideband dual-channel receiver for a pair of independent satellite multi-connectivity links with CCI and/or XPI. This non-data-aided and non-decision-directed method simultaneously processes the samples on both channels after the corresponding analog-to-digital converters (ADCs) and uses the correlation between the two received signals for the adaptive estimation and cancellation of the CCI and/or XPI in a blind and transparent fashion. The CLEAR method is derived in a channel model with CCI and/or XPI, including effects such as reduced XCD and/or XPD at the receiver side, depolarization due to atmospheric conditions, DFO between the two channels, and power imbalance due to independent receive antenna gains. The CLEAR method presents a successful operation in the presence of DFO, has a low computational complexity, and is suitable for very-high-rate implementations. The performance of the dual-channel receiver implementing the CLEAR method is simulated in terms of the received C/I and $C/(N+I)$, and it presents considerable energy efficiency improvements, being particularly beneficial for higher-order modulation. As a result, the CLEAR method is a practical solution to increase the data rates of the satellite air interface by the use of two independent satellite links. Moreover, it is a transparent solution applicable to both DVB and 5G waveforms, and therefore beneficial for providing flexibility of implementation in both DVB and 5G wideband dual-channel receivers.

The rest of the paper is organized as follows. Section 2 presents the system model, including the link setup with two independent satellites, the dual-channel transmission chain, and the channel modelling. Section 3 describes the derivation of the

CLEAR method for CCI and/or XPI compensation. Section 4 presents the performance evaluation results. Finally, Section 5 concludes the paper.

2 | System Model

Multi-connectivity with a pair of independent satellites to a single location on ground can double the data rate of the communication link, when using the same carrier frequency and signal bandwidth with a dual-channel receiver. Channel discrimination at the receiver side is achieved either by using two receive antennas with the same polarization on each link or by using different polarizations on each link in a PDM fashion. For example, one channel utilizes a right-hand circular polarization (RHCP), alternatively a vertical polarization (VP), and the other channel utilizes a left-hand circular polarization (LHCP), alternatively a horizontal polarization (HP). The imperfect decoupling of the two signals at the receive antenna in each channel introduces interference from one signal into the other. As a result, the performance of the dual-channel receiver is degraded, and an interference compensation method is required. In this section, the link setup with two independent satellites, the dual-channel transmission chain, and the channel modelling are presented.

2.1 | Link Setup With Two Independent Satellites

The use cases for realization of multi-connectivity with a pair of independent satellites to a single location on ground are presented in Figure 1. First, a setup with two steerable receive antennas at the ground location, respectively tracking each satellite, is considered, where the XCD is provided by the receive antenna patterns, and the same polarization is used on the two links. In case the satellite separation in space is very low due to a high-density mega-constellation, and the paths to the two satellites are close within the main lobe of each antenna pattern, resulting in a low XCD, PDM can be used in the setup with two receive antennas, where different polarizations are used on the two links. Second, a setup with a single steerable dual-polarization receive antenna is also considered, where different polarizations are used on the two links, and channel separation is provided in the form of XPD. In these use cases, due to the two independent satellite links, the signals are assumed to be crossed at the receiver side, and reduced XCD and/or XPD result in CCI and/or XPI. In general, these use cases are representative for the user/service downlink or the feeder downlink, even though the equivalent setup can also be considered onboard one satellite equipped with a dual-channel receiver serving two uplinks from independent ground locations.

In these two use cases, the distance between the two independent satellites, ranging from co-location to large separation, can result in different receive antenna gains on the two paths as show in Figure 1. This, in addition to the difference in slant range, can result in a difference in the received signal power, and therefore power imbalance, between the two channels at the receiver. In the case with two receive antennas on ground without PDM, the difference in the receive antenna gain on the intended and interfering paths directly results in XCD. If PDM is also used in this scenario, this XCD, when combined with the XPD, enhances the overall channel discrimination. The higher the satellite separation distance, the higher the XCD, the lesser the CCI and the need for compensation. Here, the difference in slant range on the two intended paths results in power imbalance between the channels. The higher the satellite separation on one side of the zenith, the higher the power imbalance. In the case with one receive antenna on ground with PDM, the difference in the receive antenna gain on the two intended paths results in power imbalance between the two channels. Here, the higher the satellite separation distance on one side of the zenith, the higher the power imbalance between the two channels. For example, if one satellite is at 30° elevation, while the other satellite is at 90° elevation, the doubled slant range at 30° as compared to 90° results in a 6-dB power imbalance. The power imbalance is 3 dB, if one satellite is at 45° elevation, while the other satellite is at 90° elevation.

In general, parabolic antennas have wider beams at lower frequencies and narrower beams at higher frequencies. The half-power beamwidth (HPBW) of a 70-cm parabolic dish antenna in Ka band at 20 GHz is 1.5°, following the known relation, $\text{HPBW} = 70\lambda/d$, where λ is the wavelength and d is the antenna diameter. Put into perspective, a satellite separation of 1.5° is

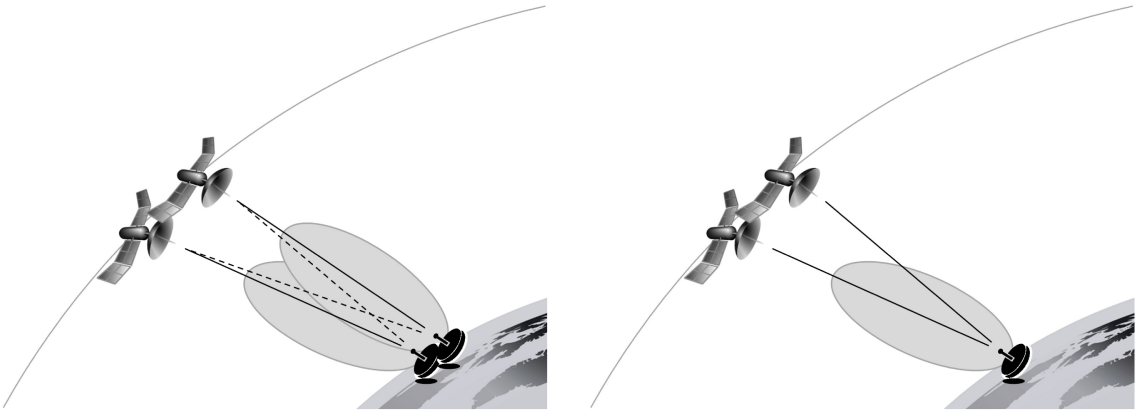

(a) Two receive antennas with or without PDM. (b) One receive antenna with PDM.

FIGURE 1 | Multi-connectivity with a pair of independent satellites to a single location on ground with two and one receive antennas.

approx. 49 km at 600-km LEO altitude, given a resulting 180° visibility arc of approx. 5840 km. Since 49-km satellite separation is quite large in the context of dense mega-constellations, it is likely that two neighboring satellites are well within the main lobe of a receive antenna on ground, resulting in reduced XCD and therefore CCI, when using the same carrier frequency and signal bandwidth on the two channels.

Regarding the carrier frequencies and the corresponding available signal bandwidths for use with a wideband dual-channel receiver, the DVB-S2X [3] and CCSDS [4] standards allocate signal bandwidths up to 500 MHz in the Ka-band downlink around 20 GHz, using mechanically or electronically steered directional antennas for very-small-aperture terminals (VSATs) on ground with linear or circular polarizations. In 5G NTN, VSATs are allocated signal bandwidths up to 800 MHz in the Ka-band downlink around 20 GHz, using mechanically or electronically steered directional antennas with circular polarizations according to Release 15 [5]. In Release 18 [16], also user equipments (UEs) are assigned similar bandwidths and antenna types in Ka band. Handheld UEs are allocated signal bandwidths up to 20 MHz in the S-band downlink around 2 GHz, using linear polarizations and omnidirectional antennas according to Release 15 [5], and the signal bandwidths are extended to 30 MHz in Release 18 [17].

Lastly, satellite communication systems which use two linear polarizations for transmission in a PDM fashion, that is, VP and HP, experience an angular shift of the polarization vectors with respect to the reference at the receive antennas, known as Faraday rotation [18]. This effect does not concern circularly polarized waves, that is, RHCP and LHCP, and is more prominent at lower frequencies, for example, below 10 GHz. The Faraday rotation is predictable and can be compensated either at the transmitter or receiver side. If not compensated, this effect results in a linear combination of the VP and HP at the receiver side and introduces XPI similar to the XPD effect, which has been previously studied in [7]. The following Faraday rotation values have been reported in [18]: 12° at 3 GHz, resulting in XPD of approx. 10 dB, and 1.1° at 10 GHz, resulting in XPD of approx. 15 dB.

In summary, at low frequencies, that is, S band, UEs have omnidirectional antennas and require PDM on two linear polarizations to realize a simultaneous downlink from two independent satellites. Lower XPD is expected, if the Faraday rotation remains uncompensated. At higher frequencies, that is, Ka band, VSATs and UEs have directional antennas and can realize a simultaneous downlink from two independent satellites at a higher satellite separation distance. At lower satellite separation distance, PDM on two circular polarizations can be required to provide channel separation.

2.2 | Dual-Channel Transmission Chain

The block diagram of a dual-channel satellite communication system is presented in Figure 2. At the transmitter side, each independent transmitter generates a stream of data bits which are encoded by means of a forward error correction (FEC) scheme, and mapped to symbols from a given modulation format. Low-density parity check (LDPC) codes are commonly employed in DVB-S2X [3] and 5G NTN [5], while CCSDS [4] relies on turbo codes. Amplitude and phase shift keying (APSK) is the modulation of choice in DVB-S2X and CCSDS, while quadrature amplitude modulation (QAM) is used in 5G NTN. The modulated symbols are grouped in physical-layer (PL) frames, and scrambled by different scrambling sequences, in order to ensure the decorrelation of the two channels. In DVB-S2X and CCSDS, the frames are then oversampled by a chosen oversampling factor and pulse shaped by means of a square root raised cosine filter (SRRCF) to generate the transmission waveform. In 5G NTN, the frames are subjected to an inverse fast Fourier transformation (IFFT) to generate the OFDM waveform. After digital-to-analog conversion (DAC), the signals are up-converted to the carrier frequency, for example, in S or Ka band, and amplified for transmission over the channel with CCI and/or XPI.

At the dual-channel receiver on ground, the signals of the channels are amplified by means of low-noise amplifiers, and they are distorted by additive white Gaussian noise (AWGN). Each signal is downconverted to baseband, and passed through an ADC. Next, the CLEAR method studied in this paper is applied

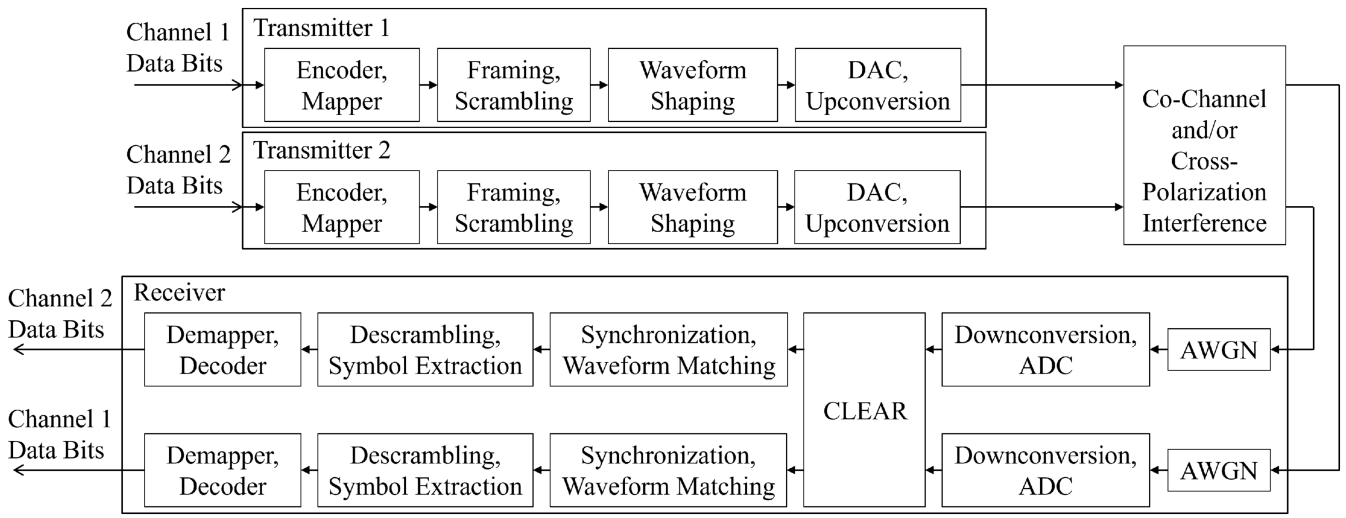

FIGURE 2 | Block diagram of the dual-channel transmission chain.

jointly to the two received signals, in order to compensate the CCI and/or XPI. After fine frequency and timing synchronization, the received waveforms are processed independently in each channel. In DVB-S2X and CCSDS, the waveform is matched filtered and downsampled to obtain the received PL frames. In 5G NTN, the OFDM waveform is subjected to a fast Fourier transformation (FFT) to produce the received PL frames. Next, the PL frames are descrambled and the received symbols extracted. These are then demapped and decoded to obtain the received data bits.

2.3 | Channel Modelling

The channel model used in this study is representative for both CCI and XPI impairments. The CCI effects include the imperfect XCD due to the reduced separation of the intended and interfering paths within the receive antenna pattern. The XPI effects include the imperfect XPD of the receive antenna, and the depolarization due to atmospheric conditions [3, 4] such as the hydrometeor-induced cross-polarization in the atmospheric propagation channel [19]. For example, the XPI in satellite links for Earth observation [3, 4] is higher at higher frequencies and at lower elevation angles due to a longer propagation path through the atmosphere, whereby an XPD down to 17 dB can be expected for Ka-band links [3]. In the use case with two receive antennas with or without PDM from Figure 1, the difference in the antenna gains on the intended and interfering paths is added to the XPD to obtain the cumulative XCD. In the use case with a single receive antenna with PDM, the cumulative XCD is given by the XPD.

The signals of the two channels consist of two respective streams of digital samples over time. At the receiver, after the two ADCs, the samples in each of the two streams are stored in shift-register buffers of N samples, where $n = 1, \ldots, N$ is the sample index, and the buffer size N is an even number. Since signal crossing at the receiver side is assumed in this work, the current pair of output signals after the channel with CCI and/or XPI, $p_1[n]$ and $p_2[n]$, can be expressed in terms of the input signals before the channel, $x_1[n]$ and $x_2[n]$, as follows:

$$p_1[n] = x_1[n] + A_\xi \exp(i\phi_\xi) x_2[n], \tag{1}$$

$$p_2[n] = \left(x_2[n] + A_\xi \exp(i\phi_\xi) x_1[n]\right) \exp(i\phi_{\mathrm{DPO}}), \tag{2}$$

where the real-valued linear amplitude, A_ξ, of the complex-valued cross factor, ξ, is related to the cumulative XCD in the channel as $\mathrm{XCD[dB]} = 10\log_{10}\left(1/A_\xi^2\right)$, ϕ_ξ is the phase angle of the cross factor ξ, accounting for depolarization due to rain and ice in the atmosphere [20], and i is the imaginary unit. The differential phase offset (DPO) between the two channels, ϕ_{DPO}, is defined as a function of the DFO phase increment at every sample as follows: $\phi_{\mathrm{DPO}} = 2\pi n f_{\mathrm{DFO}}/f_s + \phi_0$, where f_{DFO} is the DFO, f_s is the sampling rate, and ϕ_0 is a residual phase offset between the channels. Memory effects due to frequency selectivity of the XPD have been shown to have a negligible impact [7], and therefore are omitted in the channel model. The power profile of the simulated channel impulse response in [7] is very close to the 5G NTN tapped delay line D (TDL-D) [5] which is for line-of-sight (LOS) dominated conditions, similar to the use cases in Figure 1 considered in this work.

A common channel effect in the transmission from a LEO satellite to ground is the Doppler frequency shift due to the high satellite velocity. For a 20 GHz carrier frequency in Ka band and a LEO satellite velocity of approx. 7560 m/s at 600 km altitude, the maximum Doppler frequency shift amounts to 504 kHz. In DVB-S2X [3] and CCSDS [4], wideband carriers up to 500 MHz are used to mitigate the effect of the Doppler frequency shift in each channel. Similarly, in 5G NTN [5], the OFDM subcarrier spacing is scaled up to mitigate the Doppler frequency shift, resulting in wideband channel bandwidths up to 800 MHz per uplink and downlink in Ka band. In addition, the LEO Doppler frequency shift is predictable due to the predictable position of the satellites, and geolocation-based methods can be used for compensation at the synchronization block in each channel [21]. The Doppler frequency shift is therefore omitted in the channel model, and it can be regarded as inherent to $x_1[n]$ and $x_2[n]$ before crossing.

When using two independent frequency converters with two independent VCOs for the downconversion of the two channels, a DFO between the two received signals is introduced due to VCO instabilities. The DFO can be computed as the product of the carrier frequency and the differential sensitivity of the two VCOs in the two channels, for example, a DFO of 400 kHz can be expected in a dual-channel Ka-band satellite system using a 20-GHz carrier frequency and a typical differential sensitivity of the VCOs of 20 ppm. When using sampling rates, f_s, greater or equal to twice the sum of the symbol rate, B_s, and the DFO, the effect of the DFO can be modelled as an elementwise multiplication of the samples of one of the received signals with a rotating complex exponential with increment of $360 f_{\mathrm{DFO}}/f_s$ degrees per sample. As a result, the oversampling factor, η, and the sampling rate, $f_s = \eta B_s$, for a given symbol rate, B_s, can be chosen in accordance with the following inequality: $\eta B_s \geq 2(B_s + f_{\mathrm{DFO}})$. In a wideband satellite receiver with symbol rates up to 500 MBaud [7], practical oversampling factors are greater or equal to 2.1. The DFO can be compensated in the synchronization block in each channel. However, since the DFO modifies the information of the interference contained in each of the signals, as seen in (2), it needs to be considered in the design of interference compensation techniques.

3 | Derivation of the CLEAR Method for CCI and/or XPI Compensation

With local access to the signals on both channels, the CLEAR method processes the oversampled signals of the two channels after the ADCs in the receiver. Equal path lengths in terms of, for example, cables or copper traces between the receive antennas and the CLEAR digital processor are required to avoid differential timing offset between the two signals over this portion of the transmission chain. In addition, two equal synchronous sampling clocks are assumed to drive the two ADCs, which is readily achievable due to co-location of the digital processing electronics. The CLEAR method performs estimation and cancellation of the CCI and/or XPI in a transparent and adaptive

fashion, concurrently using the signal samples on both channels. The processed signal samples of the two channels are output and respectively fed to the subsequent receiver stages, preserving all structural signal properties.

The oversampled signals of the two polarizations, received after the corresponding ADCs and including the AWGN, can be expressed as follows:

$$y_1[n] = p_1[n] + w_1[n], \tag{3}$$

$$y_2[n] = p_2[n] + w_2[n], \tag{4}$$

where the noise samples, $w_1[n]$ and $w_2[n]$, are assumed as independent and identically distributed (i.i.d.) over the sampled bandwidth of ηB_s. Using (1–4) and the given assumption that the two signals, as well as the signals and the AWGN, are uncorrelated, the following expression can be derived:

$$\frac{E\left[y_1[n]y_2^*[n]\right]}{E\left[|p_1[n]|^2\right]+E\left[|p_2[n]|^2\right]} = \frac{\left(E\left[|x_1[n]|^2\right]\exp(-i\phi_\xi)+E\left[|x_2[n]|^2\right]\exp(i\phi_\xi)\right)A_\xi exp(-i\phi_{\mathrm{DPO}})}{\left(E\left[|x_1[n]|^2\right]+E\left[|x_2[n]|^2\right]\right)\left(1+A_\xi^2\right)}, \tag{5}$$

where $E[\,\cdot\,]$ denotes expectation, $|\cdot|$ denotes absolute value, and $(\cdot)^*$ is the complex conjugation operator. The estimates of the power levels of the noiseless part of the two received signals, $E\left[|p_1[n]|^2\right]$ and $E\left[|p_2[n]|^2\right]$, can be obtained from the received signal samples as follows [6, 7]:

$$E\left[|p_1[n]|^2\right] = E\left[y_{1,\mathrm{odd}}[k]y_{1,\mathrm{even}}^*[k]\right]\alpha, \tag{6}$$

$$E\left[|p_2[n]|^2\right] = E\left[y_{2,\mathrm{odd}}[k]y_{2,\mathrm{even}}^*[k]\right]\alpha, \tag{7}$$

where the independent noise samples in the odd and even received signal samples are averaged out, $k = 1, \ldots, N/2$, and α denotes the correction factor due to sampling which is evaluated by means of a numerical simulation of the signals. For a DVB-S2X [3]/CCSDS [4] waveform with SRRCF pulse shaping with roll-off factors between 5% and 35%, as well as for a 5G NTN [5] OFDM waveform with 2048 subcarriers, the correction factor due to sampling, α, is depicted as a function of the oversampling factor, η, in Figure 3, showing only minor variability of approx. 2%.

In case the signal crossing is at the transmitter side, for example, a dual-polarization transmit antenna as in [7], or in case of two co-located satellites, equal received signal power can be assumed for the two received signals, that is, $E\left[|x_1[n]|^2\right] = E\left[|x_2[n]|^2\right]$. Here, the expression from (5) can be reduced to

$$\frac{E\left[y_1[n]y_2^*[n]\right]}{\alpha\left(E\left[y_{1,\mathrm{odd}}[k]y_{1,\mathrm{even}}^*[k]\right]+E\left[y_{2,\mathrm{odd}}[k]y_{2,\mathrm{even}}^*[k]\right]\right)} = \frac{\cos(\phi_\xi)A_\xi}{1+A_\xi^2}exp(-i\phi_{\mathrm{DPO}}), \tag{8}$$

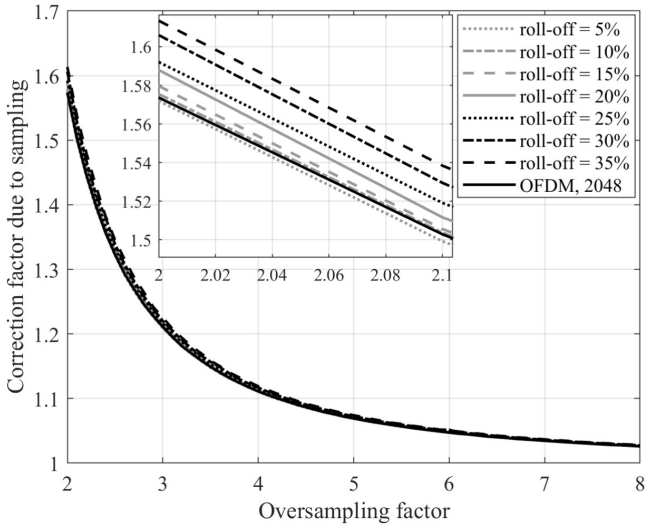

FIGURE 3 | Correction factor due to sampling as a function of the oversampling factor.

Since two equal-length co-located paths are generally assumed for the transmission in DVB-S2X [3] and CCSDS [4], the effect of the phase angle due to depolarization is generally computed as part and included in the overall XPD [3, 19], resulting in XPD down to 17 dB for Ka-band links [3]. Since the $\cos(\phi_\xi)$ in (8) is a real-valued function, the inclusion of the phase angle as part of the amplitude XPD effect [19], effectively as part of A_ξ, is justified. The effect of the phase angle up to the extreme of 45° has been studied in [7], and significant performance gains have been reported by the use of the CLEAR method under these depolarization conditions. However, when the signal crossing is at the receiver side, which is the case with two independent satellite links in this work, different signal power can be received, that is, $E\left[|x_1[n]|^2\right] \neq E\left[|x_2[n]|^2\right]$. Here, the expression from (5) remains and describes the effect of power imbalance and depolarization.

Using only the two received sample streams and the knowledge of the oversampling factor at the two ADCs, the CLEAR method employs the following complex-valued cross factor estimate between the received signals of the two polarizations [6, 7]:

$$\hat{\xi} = \mathcal{G}\left\{\frac{E\left[y_1[n]y_2^*[n]\right]}{\alpha\left(E\left[y_{1,\mathrm{odd}}[k]y_{1,\mathrm{even}}^*[k]\right]+E\left[y_{2,\mathrm{odd}}[k]y_{2,\mathrm{even}}^*[k]\right]\right)}\right\}, \tag{9}$$

where the $\mathcal{G}\{\cdot\}$ operator applies the function $g(m) = \mathrm{Real}\left\{\left(1-\sqrt{1-4m^2}\right)/(2m)\right\}$ to: (1) the amplitude of its argument (labeled as Rx 1) or (2) the real and imaginary parts of its argument (labeled as Rx 2). The function $g(m)$ is the real-value of the solution with the negative sign of the quadratic equation $mA_\xi^2 - A_\xi + m = 0$, and it is plotted in Figure 4. Since the XCD is defined as a non-negative factor in the linear domain, m is a small number between −0.5 and 0.5 in the absence of AWGN. As a result, $g(m)$ takes values between −1 and 1 which are produced by the solution with the negative sign. In the presence of AWGN,

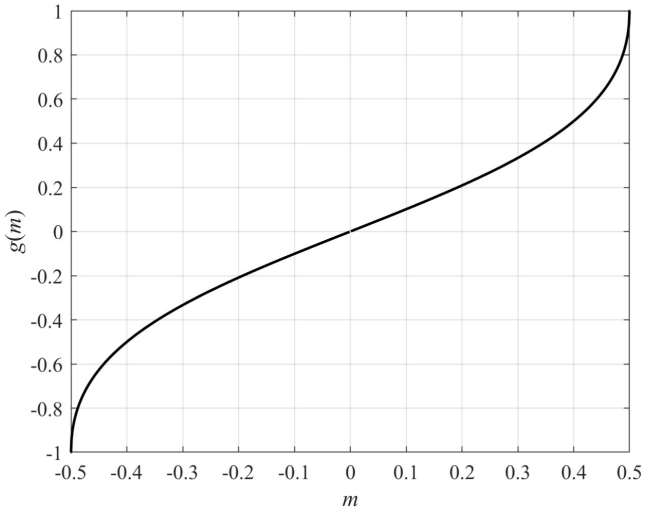

FIGURE 4 | The function $g(m)$.

m can vary outside of the range between -0.5 and 0.5, and therefore, the real value of the solution is taken to avoid numerical instability. The function $g(m)$ is quite linear for practical XCD values, that is, XCD values as low as 10 dB result in a small m, so it is almost a scaling factor. Since scaling of the amplitude and preserving the phase is equivalent to scaling the real and imaginary parts of a complex number, Rx 2 is a valid approximation of Rx 1 with a lower computational complexity for practical XCD values.

The complex-valued cross factor estimate is used in conjunction with the two received signals, $y_1[n]$ and $y_2[n]$, to compute estimates of the interference in the two channels as $\hat{\xi} y_2[n]$ and $\hat{\xi}^* y_1[n]$, respectively. The interference cancelation is performed as the elementwise subtraction of the interference estimates from the corresponding received signals, in order to produce the output signal samples of the CLEAR method as follows [6, 7]:

$$y_{1,\text{out}}[n] = y_1[n] - \hat{\xi} y_2[n], \tag{10}$$

$$y_{2,\text{out}}[n] = y_2 - \hat{\xi}^* y_1[n]. \tag{11}$$

In [6], an elaborate block diagram for the efficient implementation of the CLEAR method in a very high speed integrated circuit hardware description language (VHDL) and realization in a field programmable gate array (FPGA) chip has been presented. The size of the shift-register buffers for the received signal samples $y_1[n]$ and $y_2[n]$, N, can be selected sufficiently large to provide AWGN averaging, for example, larger than 200 samples. In the case when two independent frequency converters are used at the receiver side and there is a DFO between the two channels, the upper limit of the vector size, N, can be determined using the DFO, f_{DFO}, and the sampling rate, f_s, as $0.25 f_s/f_{\text{DFO}}$. As a result, the following inequality can be used as a guideline: $200 \leq N \leq 0.25 f_s/f_{\text{DFO}}$. Due to its low computational complexity, the CLEAR method is suitable for higher-rate applications. A hardware implementation in a wideband dual-channel satellite receiver with symbol rates up to 500 MBaud has been presented in [7], requiring a total of 104 digital signal processing (DSP) slices for real-valued multiplications at 4× parallelization which is 2% of the resources in the largest AMD Xilinx Kintex UltraScale FPGA chip.

4 | Performance Evaluation

The performance of the CLEAR method in a wideband dual-channel receiver has been evaluated by means of a Monte Carlo simulation in the transmission setup from Figure 2. The channel model includes CCI and/or XPI under LOS dominated link conditions in AWGN. Satellite transponder impairments such as linear and non-linear distortions are omitted in this study. The performance of the wideband dual-channel satellite receiver is evaluated in terms of C/I and $C/(N+I)$ at the received constellation of the used modulation format as a function of the ratio between the energy per symbol and the noise power spectral density E_s/N_0. Since the CLEAR method is transparent to the signal waveform, and it is applicable to all DVB and 5G waveforms, the symbol rate is considered as representative of the signal bandwidth in all comparisons in this study. As a result, the C/N is considered as equivalent to E_s/N_0. The $C/(N+I)$ is calculated at the received constellation as the negative value of the mean-squared error (MSE) between the received and intended symbols in dB, and the C/I is derived from the $C/(N+I)$ and E_s/N_0.

First, the performance of the two realizations of the CLEAR method, Rx 1 and Rx 2, has been compared. Here, Rx 1 applies the function $g(m)$ to the amplitude in (9), while Rx 2 applies the function $g(m)$ to the real and imaginary parts in (9) for a reduced complexity. The evaluation has been carried out in the previously studied setup from [7] to provide context for the results. For this purpose, a 500-MBaud DVB-S2X signal with a carrier roll-off of 20% in conjunction with an oversampling factor of 2, resulting in a sampling rate of 1 Gsps, has been simulated. A signal waveform consisting of 1000 physical layer (PL) frames is employed in each channel, where each PL frame consists of 10800 data symbols from a 16-APSK modulation format according to a 4/5-rate LDPC code. It should be noted that very similar performance curves resulted from tests with any modulation orders from QPSK up to 256-APSK as in [7], since the CLEAR method is transparent to the used modulation format. Cumulative XCD values of 15 and 10 dB have been selected, in order to assess the impact of the low cumulative XCD, that is, higher interference. In addition, DFOs with phase increments of 0.06°, 0.12°, and 0.18° per sample, corresponding to DFOs of 166, 333, and 500 kHz, have been considered, in order to assess the impact of the DFO between the two channels and the capability of the CLEAR method to operate in the presence of DFO. While in a practical system a minimum oversampling factor of 2.1 is used to accommodate the frequency offsets and to allow for subsequent compensation, the performance of the setup in this simulation, using an oversampling factor of 2 and assuming ideal compensation of the frequency offsets at the synchronization block, is considered very close to the performance of the practical system. In general, a higher oversampling factor results in better performance in the presence of DFO, since a higher oversampling factor directly decreases the DFO phase increment per sample, and similar performance improvements can be observed as in [7] when reducing the DFO.

One further setup parameter is the correction factor due to sampling and its low variability for the different waveforms from

Figure 3. Because of this low variability, the curves have been averaged and the resulting single value for a given oversampling factor has been reported in a table in [6, 7] for use with all the considered waveforms. It is of interest, however, to evaluate the impact of this design decision on the performance of the receiver. For this purpose, Rx 1 has been assigned the exact value of the correction factor due to sampling of 1.5985 in the considered setup, and Rx 2 uses the average tabulated value of 1.5885. In addition, another realization of Rx 2, labeled Rx 3, has been given the lowest value of the correction factor due to sampling of 1.5719 for an oversampling factor of 2, in order to evaluate the influence of this maximum 2% error on the performance of the receiver.

The resulting C/I at the receiver is presented as a function of the E_s/N_0 in Figure 5 and Figure 6 for cumulative XCD values of 15 and 10 dB, respectively. The results for Rx 2 are identical with the ones reported in [7], and therefore transferable

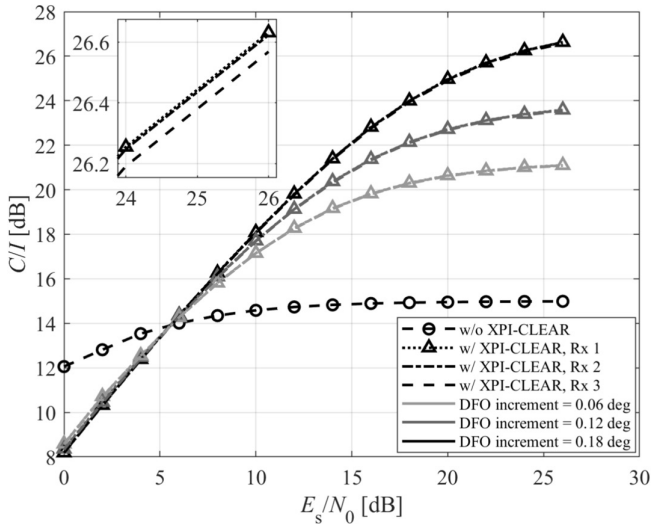

FIGURE 5 | Comparison of the C/I as a function of E_s/N_0 for an XCD of 15 dB and a DFO with phase increments of 0.06°, 0.12°, and 0.18°.

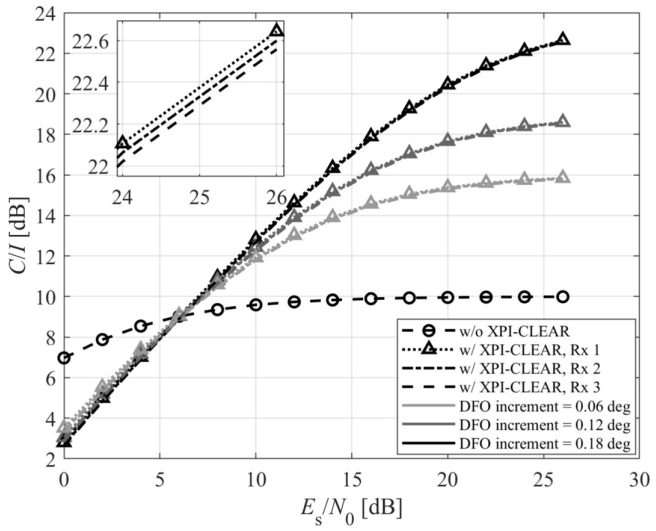

FIGURE 6 | Comparison of the C/I as a function of E_s/N_0 for an XCD of 10 dB and a DFO with phase increments of 0.06°, 0.12°, and 0.18°.

to the achievable $C/(N+I)$, reported in [7] but omitted here for the sake of brevity. The results confirm the capability of the CLEAR method to operate in the presence of DFO, producing significant energy efficiency improvements. The C/I gains of Rx 2 at midrange E_s/N_0 of 14 dB are 6.6, 5.6, and 4.4 dB for an XCD of 15 dB for the respective DFO phase increments of 0.06°, 0.12°, and 0.18° per sample. These increase to 11.7, 8.6, and 6.1 dB at higher E_s/N_0 of 26 dB. For the lower XCD of 10 dB, the C/I gains at midrange E_s/N_0 of 14 dB are 6.4, 5.3, and 4 dB, and these increase to 12.6, 8.6, and 5.8 dB at higher E_s/N_0 of 26 dB. Similarly as in [7], the improvements are achieved for E_s/N_0 values between approx. 6 and 26 dB, corresponding to the practical range for ACM with multi-level modulation.

Overall, the three studied realizations of the CLEAR method, Rx 1, Rx 2, and Rx 3, achieve very similar performance. Given the shape of the function $g(m)$, a slightly better performance is expected for Rx 1 as compared to Rx 2 for lower XCD values, that is, higher m values. For the practical range of XCD down to 10 dB, however, the improvement is merely 0.05 dB and negligible for the higher XCD of 15 dB. In addition, the 2% error in the correction factor due to sampling in Rx 3 results in a 0.05 dB degradation as compared to Rx 2. These results justify the use of the lower-complexity Rx 2 over Rx 1 with a single tabulated value for the correction factor due to sampling from [6, 7], and prove the applicability of the CLEAR method to all the considered waveforms in a transparent fashion.

As a second step of the performance evaluation, the impact of power imbalance between the channels has been studied, and the Rx 2 realization of the CLEAR method is applied in the wideband dual-channel receiver. Differences between the received signal power on the two paths of 0, 3, and 6 dB have been evaluated, that is, for co-location or symmetric positions around 90° elevation, for satellites at 45° and 90° elevation, and for satellites at 30° and 90° elevation, that is, close to the maximum power imbalance due to a difference in slant range, respectively. For this purpose, two realizations of the transmission setup have been considered, that is, one waveform representative of a DVB-S2X/CCSDS use case in Ka band and another waveform for a 5G NTN use case in S band. In the first case, a 500-MBaud signal with a carrier roll-off of 20% in conjunction with an oversampling factor of 2, resulting in a sampling rate of 1 Gsps, has been simulated. Here, a cumulative XCD of 15 dB has been selected as representative for a Ka-band transmission. For a differential sensitivity between the VCOs in the two channels of 20 ppm, a DFO of 400 kHz is obtained for a 20-GHz carrier frequency, resulting in a DFO phase increment of 0.144° per sample. In the second case, a 30-MBaud OFDM waveform with 2048 subcarriers in conjunction with an oversampling factor of 2, resulting in a sampling rate of 60 Msps, has been simulated. Here, a cumulative XCD of 10 dB has been selected as representative for an S-band transmission. For a differential sensitivity between the VCOs in the two channels of 20 ppm, a DFO of 40 kHz is obtained for a 2-GHz carrier frequency, resulting in a DFO phase increment of 0.24° per sample. For the operation of the CLEAR method, the buffer length is set to $N = 250$ which is in the middle of the range $200 \leq N \leq 0.25 f_s/f_{DFO}$ for the considered DFO phase increments.

The resulting C/I and the $C/(N+I)$ at the receiver are presented as a function of the E_s/N_0 in Figures 7 and 8 for the use cases in Ka and S band, respectively. The C/I gains at midrange E_s/N_0 of 14 dB are 5.8, {7.5, 5.9}, and {9.2, 6.1} dB for a cumulative XCD of 15 dB, for the {weaker, stronger} channel, and for power imbalances of 0, 3, and 6 dB, respectively. These increase to 9.6, {10.1, 9.7}, and {11, 10.2} dB at higher E_s/N_0 of 26 dB. The $C/(N+I)$ gains at midrange E_s/N_0 of 14 dB are 1.8, {3.1, 1.8}, and {4.8, 1.8} dB. These increase to 7.5, {8.8, 7.6}, and {10.1, 7.9} dB at higher E_s/N_0 of 26 dB. For the lower cumulative XCD of 10 dB, the C/I gains at midrange E_s/N_0 of 14 dB are 5.2, {6.7, 5.1}, and {7.8, 4.9} dB, and these increase to 8.3, {8.7, 8}, and {9, 7.6} dB at higher E_s/N_0 of 26 dB. The $C/(N+I)$ gains at midrange E_s/N_0 of 14 dB are 3, {4.6, 3}, and {6.2, 2.9} dB. These increase to 7.7, {8.3, 7.5}, and {8.8, 7.2} dB at higher E_s/N_0 of 26 dB. The presented improvements by the use of the CLEAR method overcome the penalty of the power imbalance on the weaker channel. In the case of 6-dB power imbalance, the CLEAR method even elevates the $C/(N+I)$ of the weaker channel above the $C/(N+I)$ of the case with equal-power channels without interference compensation, which can be considered the standard co-located dual-polarization scheme, and provides the flexibility of independent multi-connectivity links at higher data rates as compared to the standard solution. As a result, these $C/(N+I)$ improvements enable the application of a wider range of higher-order modulation schemes in the wideband dual-channel receiver for LEO satellite multi-connectivity with independent links.

As a last step of the performance evaluation, also the effect of the phase angle accounting for depolarization due to rain and ice in the atmosphere [19, 20] has been included in the simulation setup with power imbalance. For this purpose, a higher phase angle of 10° and a lower phase angle of 5° has been considered corresponding to practical values of higher depolarization in Ka band and lower depolarization in S band [19]. The resulting C/I at the receiver is presented as a function of the E_s/N_0 in Figure 9

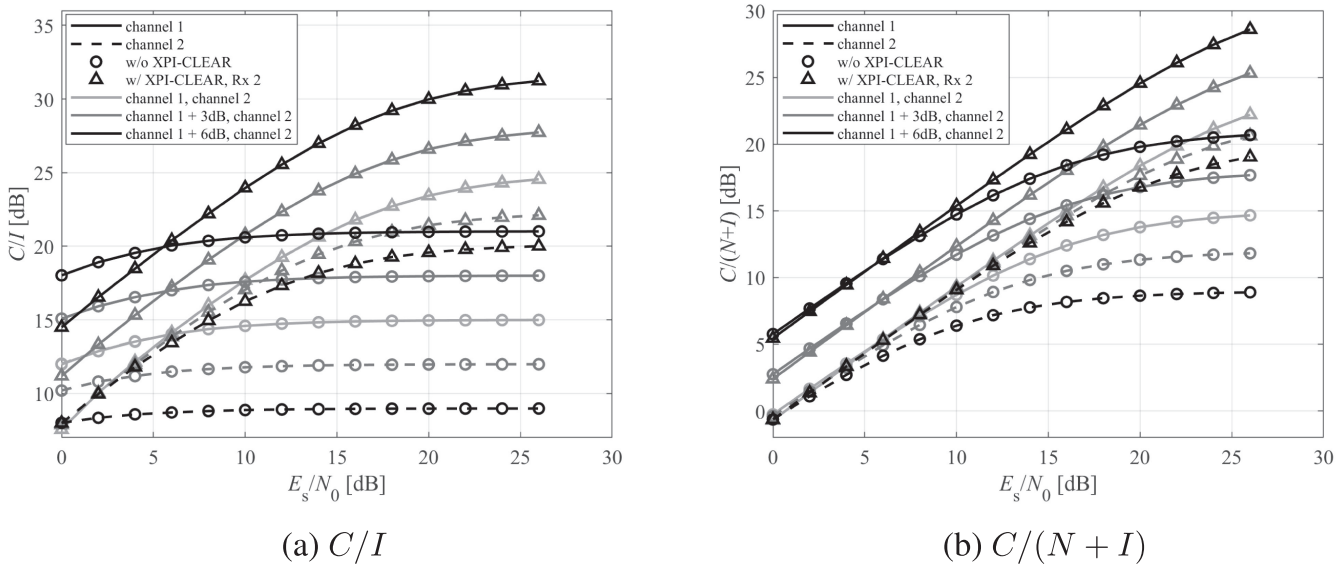

FIGURE 7 | Comparison of the received power ratios as a function of E_s/N_0 for an XCD of 15 dB and channel imbalance of 0, 3, and 6 dB.

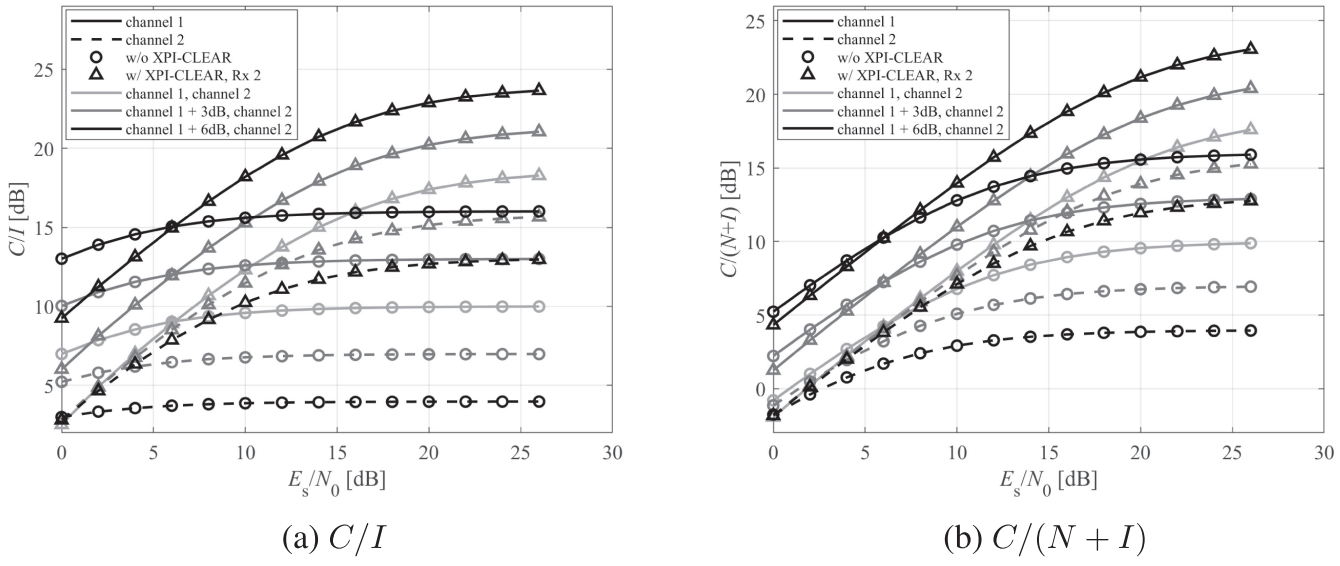

FIGURE 8 | Comparison of the received power ratios as a function of E_s/N_0 for an XCD of 10 dB and channel imbalance of 0, 3, and 6 dB.

and Figure 10 for the use cases in Ka and S band, respectively. The C/I gains at midrange E_s/N_0 of 14 dB are 5.4, {7.3, 5.1}, and {9.1, 5} dB for the cumulative XCD of 15 dB, for phase angle of 10°, for the {weaker, stronger} channel, and for power imbalances of 0, 3 and 6 dB, respectively. These increase to 8.5, {9.6, 7.9}, and {10.8, 7.6} dB at higher E_s/N_0 of 26 dB. For the lower cumulative XCD of 10 dB and phase angle of 5°, the C/I gains at midrange E_s/N_0 of 14 dB are 5.1, {6.6, 4.9}, and {7.8, 4.6} dB, and these increase to 8.1, {8.6, 7.7}, and {8.9, 7.1} dB at higher E_s/N_0 of 26 dB. The inclusion of the depolarization phase angle results in only minor degradation of the weaker channel of up to 0.5 dB at the expense of up to 2.6-dB degradation of the stronger channel in Ka band, nonetheless presenting considerable improvements. In S band, the channels experience only a minor degradation of up to 0.1 and 0.5 dB, respectively.

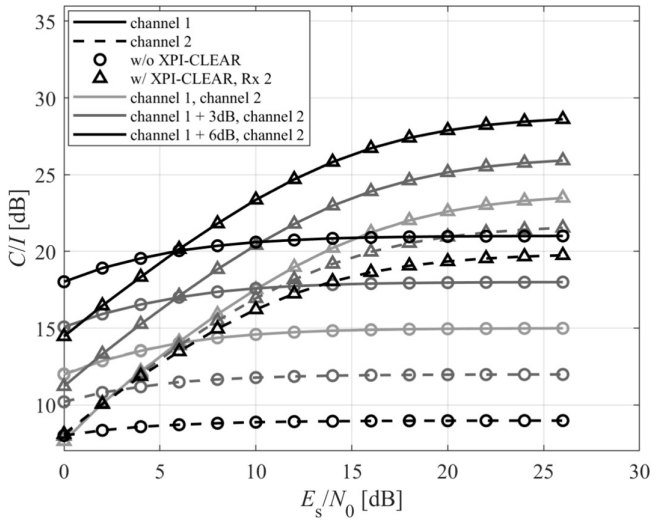

FIGURE 9 | Comparison of the C/I as a function of E_s/N_0 for an XCD of 15 dB, a DFO phase increment of 0.144°, depolarization phase angle of 10°, and channel imbalance of 0, 3, and 6 dB.

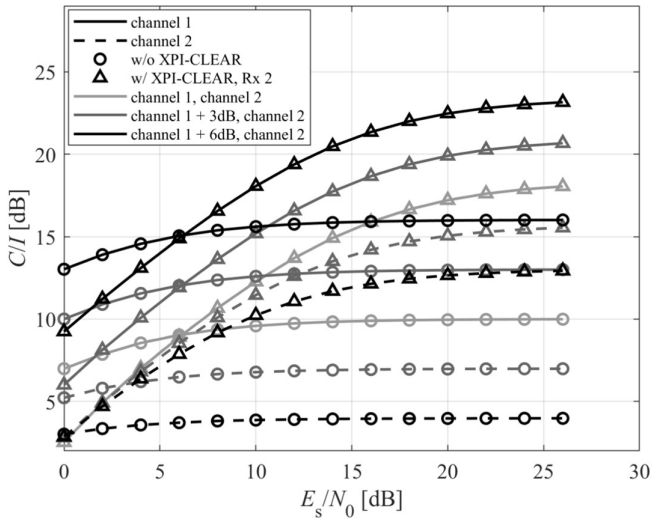

FIGURE 10 | Comparison of the C/I as a function of E_s/N_0 for an XCD of 10 dB, a DFO phase increment of 0.24°, depolarization phase angle of 5°, and channel imbalance of 0, 3, and 6 dB.

Overall, the presented considerable improvements in energy efficiency and the enabled use of higher order modulation with practical cumulative XCD values down to as low as 10 dB in the presence of all the considered channel effects show that the CLEAR method is a practical solution to increase the energy efficiency of the air interface. Therefore, the implementation of the CLEAR method in a wideband dual-channel receiver can increase the data rate of the satellite link by reducing the interference and enabling the use of two independent satellite multi-connectivity links.

5 | Conclusion

In this paper, the adaptive, blind and transparent CLEAR method has been presented for application in a wideband dual-channel receiver for a pair of independent satellite multi-connectivity links. Use cases for the realization of this setup have been described with or without PDM, using the same carrier frequency and signal bandwidth with increased CCI and/or XPI. Positioned after the ADCs of the two channels in the wideband receiver, the CLEAR method for adaptive interference estimation and compensation has been derived in a channel model, including effects such as reduced XCD and/or XPD at the receiver side, depolarization due to atmospheric conditions, DFO between the two channels, and power imbalance due to independent receive antenna gains. The C/I and $C/(N+I)$ performance of the receiver with the CLEAR method has been evaluated, and significant energy efficiency improvements have been presented with all the considered channel effects. This low-complexity high-rate interference compensation method enables the use of higher-order modulation even in very low XCD of 10 dB by increasing the $C/(N+I)$ up to the range around 20 dB. As a result, the CLEAR method is a practical solution that enables the use of two independent satellite multi-connectivity links by successfully mitigating the interference, resulting in an increase of the data rate of the satellite air interface. Being a transparent solution applicable to both DVB and 5G waveforms, the CLEAR method provides the flexibility of implementation in both DVB and 5G wideband dual-channel receivers.

Acknowledgments

Open Access funding enabled and organized by Projekt DEAL.

Conflicts of Interest

The authors declare no conflicts of interest.

References

1. United States Government Accountability Office, "Report to Congressional Addressees, Technology Assessment, Large Constellations of Satellites, Mitigating Environmental and Other Effects," 2022.

2. ESA Space Debris Office, "ESA's Annual Space Environment Report," 2025.

3. "Implementation Guidelines for the Second Generation System for Broadcasting, Interactive Services, News Gathering and Other Broadband Satellite Applications; Part II: S2-Extensions (DVB-S2X)," ETSI TR 102 376–2, 2015.

4. "Flexible Advanced Coding and Modulation Scheme for High Rate Telemetry Applications," CCSDS 131.2-B-1, 2012.

5. 3rd Generation Partnership Project (3GPP); "Technical Specification Group Radio Access Network; Study on New Radio (NR) to Support Non-Terrestrial Networks (Release 15)," Technical Report 3GPP TR38.811, 2020.

6. S. Dimitrov "Method for Receiving Two Digital Signals in a Dual-Polarization Digital Communication System," WO2023/161084A1, 2023.

7. S. Dimitrov, V. Dantona, and G. Mocker, "Design and Implementation of Transparent Cross-Polarization Interference Compensation in a Wideband Dual-Polarization Satellite Receiver," *International Journal of Satellite Communications and Networking* 42, no. 6 (2024): 481–492.

8. 3rd Generation Partnership Project (3GPP); "Technical Specification Group Radio Access Network; Solutions for NR to Support Non-Terrestrial Networks (NTN) (Release 16)," Technical Report 3GPP TR38.821, 2023.

9. J. P. Millerioux, E. Peragin, H. Guillon, et al., "Preliminary Definition of a High Performance X-Band Transmitter for Microsatellites," in *Proc. of the 4S Symposium 2012* (ESA, 2012).

10. I. R. A. Bahamonde, J. M. T. Romano, and J. C. M. Mota, "On the Adaptive Filtering for Cross-Polarization Interference Canceler," in *Proc. SBT/IEEE International Symposium on Telecommunications* (IEEE, 1990).

11. M. Kawai "Cross Polarization Interference Compensation Method, and Cross Polarization Interference Compensating Device," EP1940061A1, 2008.

12. Y. Vasavada, B. Allen, B. Moores, and A. Wedisinghe, "A Proactive Adaptation of Coding and Modulation Scheme to Mitigate Adjacent System Interference in Large LEO Constellations," in *Proc. 41st International Communications Satellite Systems Conference (ICSSC 2024)* (IET, 2024).

13. M. Sellathurai, P. Guinand, and J. Lodge, "Space-Time Coding in Mobile Satellite Communications Using Dual-Polarized Channels," *IEEE Transactions on Vehicular Technology* 55, no. 1 (2006): 188–199.

14. P. Henarejos and A. I. Perez-Neira, "Dual Polarized Modulation and Reception for Next Generation Mobile Satellite Communications," *IEEE Transactions on Communications* 63, no. 10 (2015): 3803–3812.

15. K. X. Li, L. You, J. Wang, et al., "Massive MIMO Downlink Transmission for LEO Satellite Communications," in *Proc. IEEE 94th Vehicular Technology Conference (VTC2021-Fall)* (IEEE, 2021).

16. 3GPP TSG-RAN, "NR NTN (Non-Terrestrial Networks) Enhancements," NR_NTN_enh, RP-234011 (Release 18), 2023.

17. 3GPP TSG-RAN, "30 MHz Channel Bandwidth for NR NTN (Non-Terrestrial Networks) in FR1, NR_NTN_CBW_30MHz-Core, RP-232647 (Release 18)," 2023.

18. W. L. Flock, *NASA-RP-1108: Propagation Effects on Satellite Systems at Frequencies Below 10 GHz, a Handbook for Satellite Systems Design*, 1st ed. (National Aeronautics and Space Administration, 1983).

19. "Propagation Data and Prediction Methods Required for the Design of Earth-Space Telecommunication Systems," ITU-R P.618–13, 2017.

20. W. P. Overstreet, C. W. Bostian, "The Phase of the Crosspolarized Signal Generated by Millimeter Wave Propagation Through Rain," NASA-CR-159894, 1978.

21. B. H. Yeh, J. M. Wu, and R. Y. Chang, "Efficient Doppler Compensation for LEO Satellite Downlink OFDMA Systems," *IEEE Transactions on Vehicular Technology* 73, no. 12 (2024): 18,863–18,877.